Calibrating an optical fiber humidity sensor and applying it in real-time monitoring of relative humidity in fresh concrete

Xiaokang Zhang (张小康)[*], **Zhuoyong Deng (邓焯泳), and Hanlang Xu (许瀚朗)**

Department of Physics, School of Science, South China University of Technology, Guangzhou 510640, China

[*]*Corresponding author: xkzhang@scut.edu.cn*

A doubly cladding single-mode fiber humidity sensor is fabricated by agarose. The sensor has an insertion loss of −0.08 dB and a power change of −17.83 dB. The responses of the sensor to a relative humidity (RH) range form 30% to 100% at a temperature range form 25 to 34 °C are validated. The experiments demonstrate that the absorbability of agarose gel to moisture decreases with increasing RH in measured gas. We propose a calibration method that uses lookup tables and construct a corresponding calibration matrix. Using the sensor, we conduct real-time monitoring of RH in fresh concrete during its hardening process.

OCIS codes: 060.2370, 120.4820.

doi: 10.3788/COL201311.090604.

Humidity has a significant effect on many industries, such as textile manufacture, medical production, and national defense. Optical fiber humidity sensors can overcome many limitations of electrical sensors, such as electromagnetic interference and the inability to measure humidity near 100% relative humidity (RH). Thus, optical fiber systems that monitor humidity present extensive development prospects.

Optical fiber approaches for humidity sensing are based primarily on optical power variations[1−5] and wavelength shifts[6−8]. Each method has its own advantages. Wavelength-based sensors have excellent long-term stability, but optical power interrogation is simpler and more economical than complex spectroscopy. Therefore, an optical fiber sensing scheme based on power variations would be of great value in short-term detection applications, such as the monitoring of humidity in fresh concrete during its hardening process. The fashions of power-based sensers include evanescent field sensors and other differentially structured sensors, such as tilted fiber Bragg grating (FBG)[4] and combined FBG and tapered fibers[5]. The structure of evanescent field sensors comprises doubly clad single-mode fibers (DCSMF)[1], tapered fibers[2], and side-polished fibers[3]. Among the power variations obtained in these sensors, those derived in a DCSMF sensor reaches nearly 9 dB at 30% to 100% RH and 25 °C, with an insertion loss of less than −0.5 dB[1].

RH is defined as the ratio between actual water vapor pressure in measured gas and the saturation water vapor pressure (P_S) at the same gas temperature. P_S can be calculated by an empirical function thus[9]

$$P_{\mathbf{S}} = 6.1078 \exp\left(17.269 \frac{T}{T + 237.3}\right). \qquad (1)$$

The performance of a humidity sensor at different temperatures should be evaluated because RH is temperature dependent. Kronenberg *et al.*[6] studied the influence of RH and temperature on an FBG. Despite the contributions of the study, however more complex investigations are required for practical applications.

Humidity sensors based on optical power variations have only been studied at a certain temperature. To the best of our knowledge, the behavior of humidity sensors at different temperatures has not been examined, and reports on the application of optical fiber humidity sensors are scarce.

In this letter, a DCSMF humidity sensor with large power variations and low insertion loss is fabricated. The responses of the sensor to 30% to 100% RH at 25 to 34 °C are verified. An approach to calibrating the optical fiber humidity sensor is also proposed. We use the humidity sensor and a temperature sensor to monitor RH in fresh concrete during its hardening process.

The principle and fabrication of DCSMF humidity sensors are described in Ref. [1]. The fiber used in our study is naked Corning SMF-28e, whose total length is around 100 cm. The sensing zone is marked approximately 2 cm from the central portion of the fiber. The original cladding of the fiber in the zone is partly removed by etching. The rest functions as an inner cladding. The etched part of the fiber is fixed onto a plate with dimensions of $7 \times 3 \times 0.2$ (cm), in which the center part is hollowed out and the sensing zone does not come into contact with the plate. Two sections of copper wires (diameter, 0.9 mm; length, 4 cm) are positioned at both sides of the zone to form two enclosures. Hydrogel compounded by agarose granules (dry) mixed with deionized water is coated onto the sensing zone to form an outer cladding. The copper wires protect the zone from damage and enable convenient coating. The optical fiber sensor is shown in Fig. 1. The sensing probe is dried at room condition for a day, and the two ends of the fiber are spliced into two pigtails by fusion.

The sensing probe is inserted into a climatic chamber (Binder KBF 115). The light from a stabilized DFB-LD light source (1 550 nm; output power, 0.08 dBm) is injected into the sensor, and the output signal is measured by an optical power meter (both provided by Accelink Technologies Co.).

Fig. 1. Optical fiber humidity sensor.
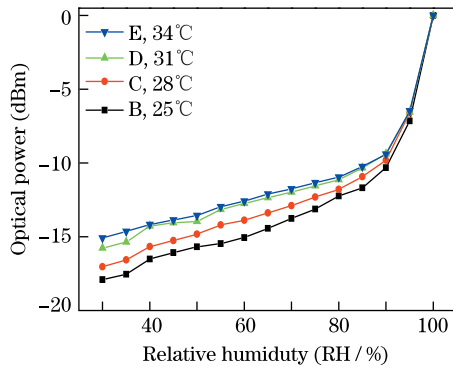
Fig. 2. Optical power losses for a DCSMF sensor versus RH in ambient air around the sensing head.

The sensing probe is subjected to wet–dry cycles to accelerate aging. The climatic chamber runs cycles at a humidity range of 30% to 90% RH at a fixed temperature of 25 °C once a day for five consecutive days. Then, the chamber is operated at a humidity range of 30% to 95% RH with intervals of 5% RH at 25, 28, 31 and 34 °C. The 5% RH intervals last 40 min. The responses of the sensor to different RH levels at different temperatures are shown in Fig. 2.

The optical power loss of the sensor decreases with increasing RH at constant temperature. Previous studies[1] demonstrated that optical power loss decreases as the water content of agarose coating increases at high RH and so the refractive index of the coating (n) decreases.

Figure 2 also shows that the loss decreases with higher temperature at constant RH. This result can be attributed to the strong saturation vapor pressure (100% RH) at high temperature and the high water content of the air in the chamber even at a constant RH. Thus, n decreases with increasing temperature and decreasing loss.

Figure 2 shows different changes in loss at the same changes of temperature under different RH conditions. For example, loss changes by 2.8 dB at a fixed humidity of 30% RH and a temperature range form 25 to 34 °C. Such change is 0.9 dB at 90% RH. Thus, the temperature responses are 0.3 and 0.1 dB/°C, respectively. However, the change in saturated vapor pressure, as calculated from Eq. (1), is approximately 2.15 kPa when temperature increases from 25 to 34 °C. The changes in absolute vapor pressure are 0.65 kPa at 30% RH and 1.94 kPa at 90% RH. Given that the temperature response at 30% RH is larger than that at 90% RH, we conclude that the absorbability of the agarose coating under moisture in high RH considerably decreases. Thus, the effect of temperature on sensor attenuation also diminishes.

Sensor attenuation at 100% RH cannot be directly detected because of the limitations of the climatic chamber. The datum at 100% RH is obtained by dripping sufficient water with corresponding temperatures on the sensing zone. A previous test shows that complete immersion of the sensor in water decreases optical power attenuation to −0.12 dBm in 1 min then the attenuation plateaus at −0.008 dBm. Given that the water content of the agarose coating in the experiment reaches its maximum, the results can be regarded as data obtained at 100% RH. Figure 2 indicates that the attenuations at 100% RH and 25 to 34 °C are almost the same; i.e., only −0.08 dBm. Sensor attenuation under saturated moisture absorption reaches a minimum value, in which case temperature minimally affects attenuation.

The characteristics of attenuation change with temperature are discussed above. Conversely, each curve in Fig. 2 shows different liner behaviors for two different humidity ranges (30%–90% RH and 90%–100% RH). At the 34 °C curve, for example, the power changes are −5.68 and −9.40 dB at 30% to 90% RH and 90% to 100% RH, respectively. The corresponding sensitivities are 9.47 and 94.0 dB/% RH, respectively.

These data suggest that the attenuation of the sensor with temperature and RH in measured gas are complex. An expression that combines RH with sensor attenuation cannot be fitted. We therefore propose a method in which lookup tables are used to calibrate the RH of the humidity sensor. A calibration matrix can be constructed and fitted on the basis of experimental data because such data are always limited. For example, the RH interval in one of our experiments is 5%. The other data, for which the RH interval is 0.1%, can be fitted from the experimental data derived from 5% RH. The temperature interval applied in this study is 2 °C and that for the fitted data can be 0.1 °C. The data for different RH values at a fixed temperature are placed on the same column. The rank data in the matrix belong to the same RH at different temperatures. Thus, a matrix (C_{ik}) with dimensions of 701×91 is built, with a resolution ratio of 0.1% RH at a range of 30% to 100% RH and 0.1 °C at a temperature range of 25 to 34 °C. The calibration matrix is shown in Fig. 3.

We monitor the evolution of RH in the fresh concrete using the calibrated humidity sensor. The cement used in our experiment is Shi Jing Composite Portland Cement P.C 32.5. Concrete is a mixture of cement, sand, and water. The mass ratio is 3.5:3:1. After these components are mixed and after part of the fresh concrete was placed in a bottle (a 6-L Sprite bottle), a thin copper board was placed on the fresh concrete to prevent the
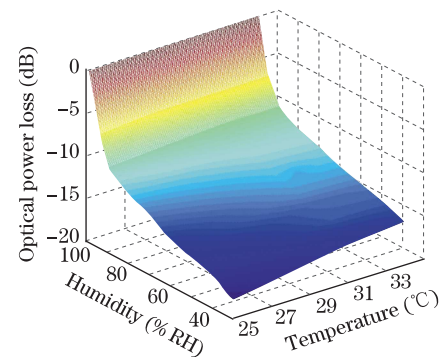
Fig. 3. Calibration matrix of a DCSMF humidity sensor used at 30% to 100% RH and 25 to 34 °C.

fibers from breaking. The humidity and a temperature fiber sensor (see Refs. [1, 10]) are placed on the board. The two sensors were then covered with the fresh concrete. A thermometer is inserted in the concrete for the calibration of the temperature sensor. The light source is equally divided into two beams by an optical splitter; the beams are then input into the two sensors. The outputs of the two sensors are detected by two optical power meters and recorded by two computers.

The fabrication of the temperature fiber sensor is reported in Refs. [1, 10]. The outer cladding material in this letter is a blend of polymers PMMA and PVDF, combined at a mass ratio of 49:51. Tests demonstrate that this temperature sensor responds not only to temperature, but also to humidity. The sensor wrapped with multiple aluminum foil continues to be affected by humidity, prompting us to calibrate the sensor with the thermometer inserted in the concrete specimen to monitor the temperature in the specimen.

Figure 4 shows the 33-h real-time optical power output from the humidity and temperature sensor. The humidity data in Fig. 4 has been deduced the insertion loss of the system. This loss is determined by the minimum loss of the humidity sensor after it is covered with fresh concrete. At the time, the water content in the agarose coating of the humidity sensor reaches the saturation level and the output of the humidity sensor corresponds to the data derived at 100% RH.

After the temperature monitoring results in Fig. 4 are calibrated with the thermometer inserted in the specimen, the findings are amplified 10-fold and rounded (A_T).
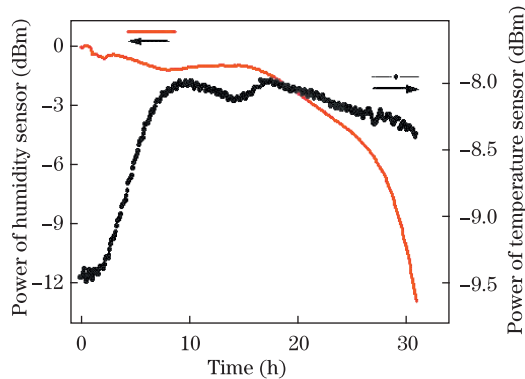
Fig. 4. Optical power outputs of a humidity sensor and a temperature sensor in the monitoring of the hardening process of fresh concrete.
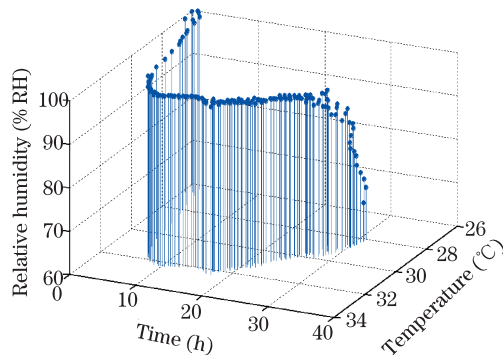
Fig. 5. Results of RH and temperature monitoring for fresh concrete during its hardening process.

A_T is used to determine the number of a column k as

$$k = A_T - 249. \qquad (2)$$

Humidity monitoring (A_H) that corresponds to the same period of an A_T is compared with the data on the k-th column in the calibration matrix. Suppose that the datum on the nearest A_H in the matrix is C_{ik} and the corresponding RH can be determined by

$$\mathrm{RH}(\%) = (i + 299)/10. \qquad (3)$$

The corresponding temperature is $A_T/10$. These calculations above can be completed by computer programming. The calibration results are shown in Fig. 5, which indicates that RH in the fresh concrete monotonically decreases from 100% to 68.9% and that the temperature initially rises from room temperature to 32.3 °C before it decreases to 28 °C during the hardening process (33 h).

In conclusion, we propose a method of RH calibration on an optical fiber humidity sensor. The calibrated sensor is used to monitor RH in fresh concrete during its hardening process, in which the resolution ratio of RH is 0.1% at a range form 30% to 100% and the resolution ratio of temperature is 0.1 °C at a range from 25 to 34 °C.

The humidity sensor reported in this letter has a DC-SMF structure. The insertion loss of the sensor is only −0.08 dB and its minimum attenuation occurs at 100% RH, which enables convenient sensor calibration. The responses of the sensor to 30%–100% RH at 25–34 °C are investigated. Power changes by −17.83 dB at 30%–100% RH and 25 °C. The absorbability of the agarose coating under moisture decreases with increasing RH in the measured gas. Thus, the effect of temperature on sensor attenuation decreases at high RH.

The calibration method proposed in this letter can be used to realize an optical fiber RH sensing system for real-time monitoring. It presents the advantages of simple calibration and low cost, making it of considerable value in practical application.

References

1. X. Zhang, X. Ye, and Z. Chen, Acta Opt. Sin. (in Chinese) **31,** 0606004 (2011).
2. L. Zhang, F. Gu, J. Lou, X. Yin, and L. Tong, Opt. Express **16,** 13349 (2008).
3. A. Gaston, I. Lozano, F. Perez, F. Auza, and J. Sevilla, IEEE Sens. J. **3,** 806 (2003).
4. Y. Miao, B. Liu, H. Zhang, Y. Li, H. Zhou, H. Sun, W. Zhang, and Q. Zhao, IEEE Photon. Technol. Lett. **21,** 441 (2009).
5. T. Li, X. Dong, C. C. Chan, C.-L. Zhao, and P. Zu, IEEE Sensors J. **12,** 2205 (2012).
6. P. Kronenberg, P. K. Rastogi, P. Giaccari, and H. G. Limberger, Opt. Lett. **27,** 1385 (2002).
7. W. Zhang, D. J. Webb, and G.-D. Peng, J. Lightwave Technol. **30,** 1090 (2012).
8. B.-M. Mao, Y. Wei, and B. Zhou, Chin. Opt. Lett. **10,** 050501 (2012).
9. E. Eccel, Meteorol. Appl. **19,** 118 (2012).
10. X. Zhang, D. Yan, S. Mo, and Z. Nong, Proc. SPIE **7508,** 750807 (2009).